

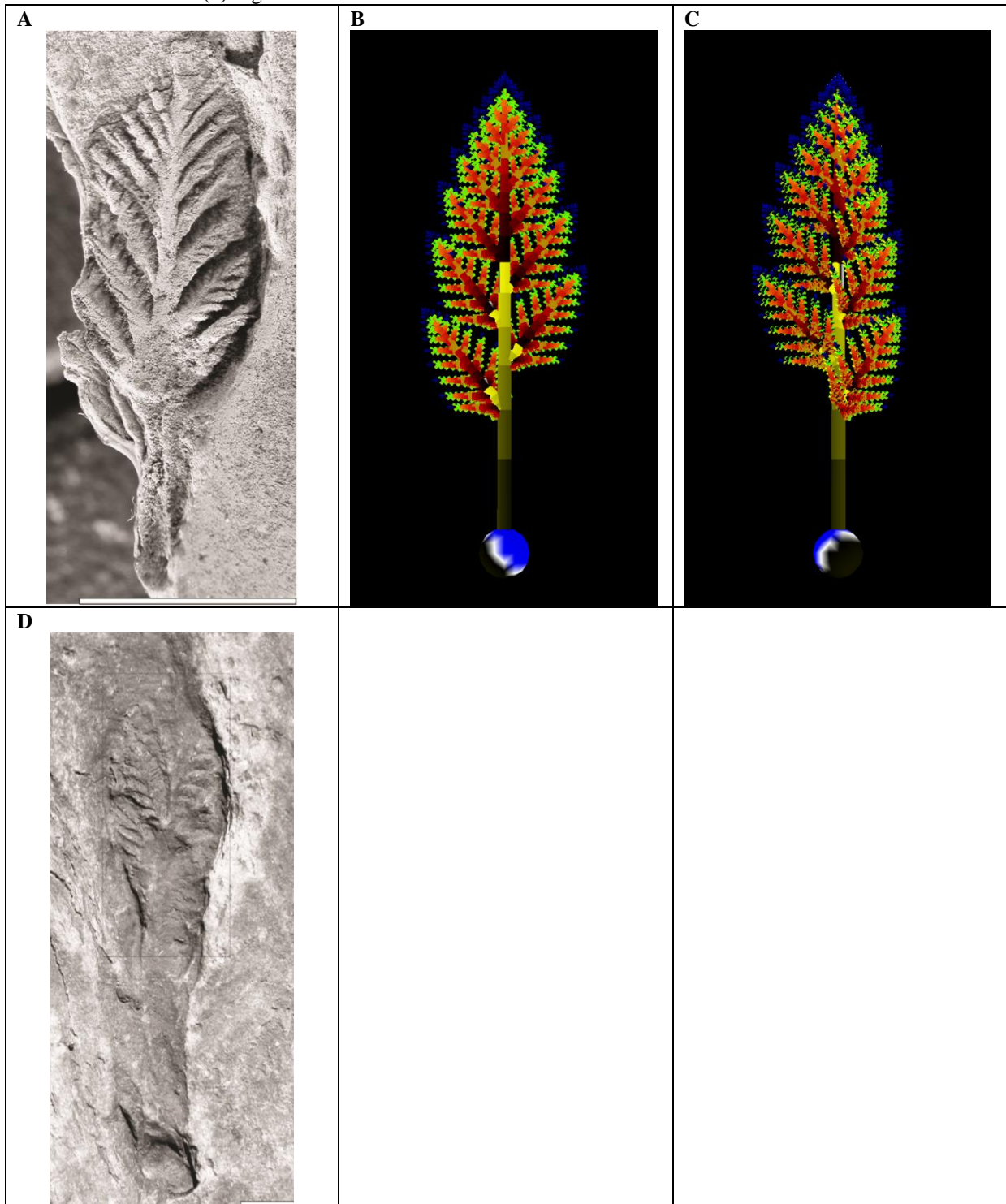
SI Appendix

Specimen analysis for L-system parameter coding

Avalofractus abaculus

Alternate, self-similar branching is visible in exceptionally preserved, three-dimensional specimens from Spaniard's Bay, Newfoundland, described by Narbonne et al. (4). Measurements taken from Fig. 3.1 of Narbonne et al. (4) were used to code y-axis branching angles for the 1st order branches (n=16 measurements gave a mean of 38°) and 2nd order branches (mean=47°, n=24). Preservation and photographic image resolution are not sufficient to allow measurement of branching angles for branches of order greater than 2. In the absence of evidence to the contrary, branches of order ≥ 3 were coded as having y-axis branching angles self-similar to those of 2nd order branches. An x-axis rotation of 15° was used to model pivoting (4) of the branches relative to their axis. The frond shape is ovate (4), with width approximately 47% of height (excluding basal stem and holdfast). Specimens preserve between four and eight imbricate primary (1st order) branches on left and right sides of the main stem (4). These interrelated morphological features were modeled using a moderate lateral branching delay and a moderate increase in lateral branch elongation rate, relative to the stem (see Table S1 for parameter values). The imprint of a bulbous holdfast (modeled as a sphere) is visible in one specimen (Fig. S1D; Fig. 3.4 of (4)). Holdfast diameter measured from this specimen is approximately 38% of maximum frond width.

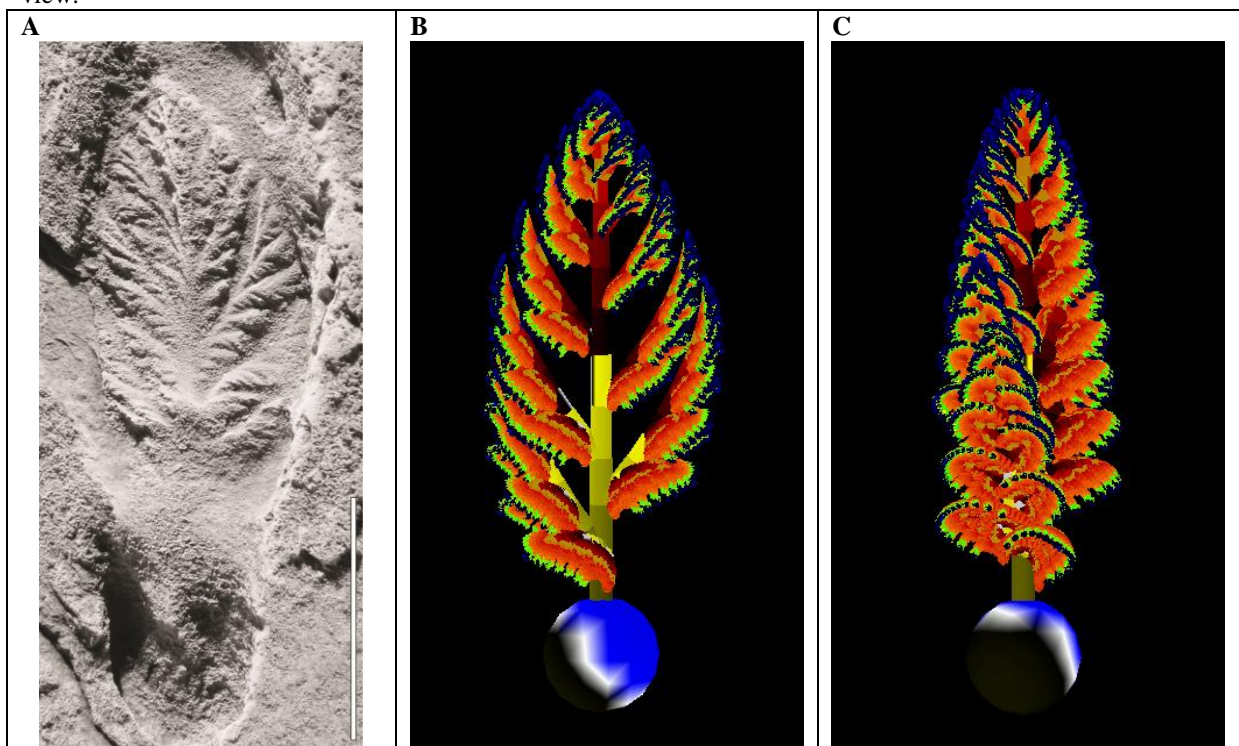
Fig. S1. *Avalofractus abaculus*. (A) Specimen from Spaniard's Bay, Newfoundland. Image reproduced with permission from Narbonne et al. (4) Fig. 3.1. Scale bar 1cm. (B) L-system model. Frontal view. Colors indicate increasing branch segment age from base to apices. (C) Rotated view. (D) Image reproduced with permission from Narbonne et al. (4) Fig. 3.4. Scale bar 1cm.



Beothukis mistakensis

Primary branches are visibly alternating. However, secondary (2nd order) branches are only visible on one side of each primary branch. This has been interpreted as the probable result of “folding” (4) or “furling” (45) of secondary branches over the primary branch axis so that one side of an alternating series is “undisplayed” (45). Here, this feature was modeled using a 90° z-axis rotation of the primary branches accompanied by a 5° x-axis curvature for branches of order ≥ 2 (giving a convex upper surface to the secondary branches). A concave upper curvature to the primary branches is visible in the exceptionally preserved specimen from Spaniard’s Bay (Fig. S2A; Narbonne et al. (4) Fig. 5.1). This was modeled using 357° x-axis curvature. Y-axis branching angles were coded based on measurements from Fig. 5.1 of Narbonne et al. (4) (1st order mean=43, n=10; 2nd order mean=46, n=10; 3rd order mean=56, n=15 used for branches order ≥ 3). A small amount of helical torsion of the stem (reported to be visible in multiple specimens (4)) was modeled using a 355° z-axis rotation (branch order 0 only). Six to nine primary branches may be visible on each side of a frond (4) and frond width was measured at approximately 54% of height. This morphology was modeled using a moderate lateral branching delay and moderate increase in lateral branch elongation rate relative to the stem (Table S1). Holdfast width was measured at approximately 64% of maximum frond width.

Fig. S2. *Beothukis mistakensis*. (A) Specimen from Spaniard’s Bay, Newfoundland. Image reproduced with permission from Narbonne et al. (4) Fig. 5.1. Scale bar 1cm. (B) L-system model. Frontal view. (C) Rotated view.

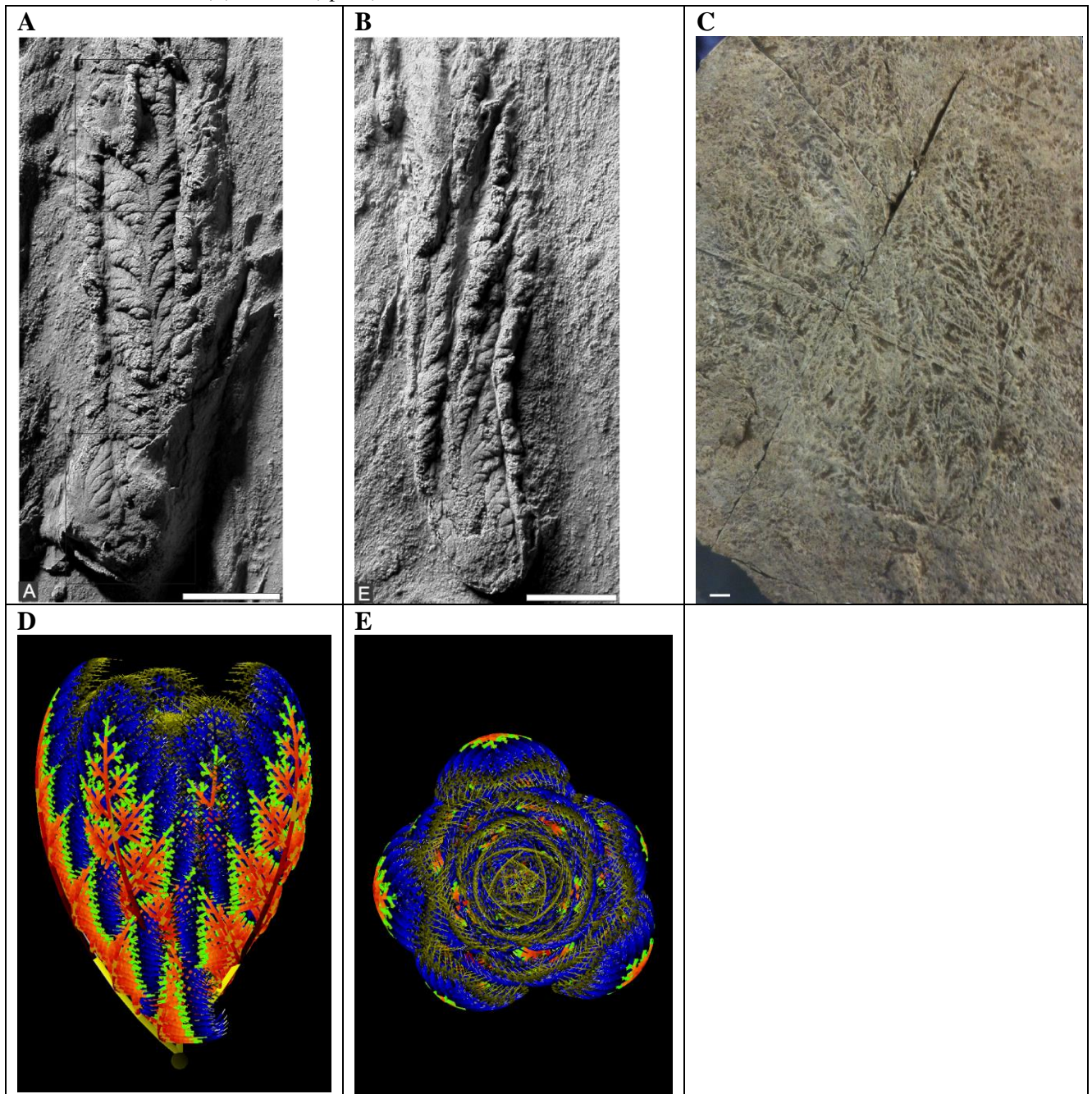


Bradgatia linfordensis

This species is known from multiple specimens from Leicestershire (Boynton & Ford, 1995 cited in (32)) and Newfoundland and has been variously described as fan (45), bush, leek, or lettuce shaped (32). Small (likely juvenile) and exceptionally preserved specimens from Spaniard’s Bay, Newfoundland (32) suggest that long branches (labelled as primary branches in the ordering series used here) emerge at close intervals from the basal region (Fig. S3A-B), with three to eight usually visible in fossil specimens (32). This arrangement is

modeled here using a very reduced elongation rate (Table S1) for the central axis, from which the primary branches emerge (Fig. S3D-E). Specimens show a variety of dimensions, from height greater than width (Fig. S3) to width greater than height (e.g. (32). Fig. 3), suggesting ontogenetic and taphonomic variability (32). Further to this, some specimens appear to have been flattened on their side (with the basal main axis at the bottom of the specimen, as in Fig. S3A-C, with specimen Fig. S3C having width approx. 66% of height), while others appear to have flattened from above, with the primary branches emanating from a central region (32). This second taphonomic class suggests that the large branches radiated from the center, through 360° (32). Here, the distribution of the primary branches is modeled using a 42.5° helical z-axis rotation around the central axis. This results in a 137.5° spacing between sequentially produced primary branches, a common natural pattern which maximizes the distance between helically distributed structures (46). The small, exceptionally preserved specimens of Spaniard's Bay (Fig. S3A-B) show very elongate primary branches, with relatively evenly sized and spaced, diamond-shaped secondary branches. The secondary branches have a moderate, convex upper curvature (Table S1). Large, presumably adult specimens from Leicestershire (e.g. Fig. S3C) also show elongate, plumose primary branches although fine details are not as well preserved. This specimen indicates a moderate concave upper curvature to the primary branches (Table S1). The plumose morphology of the primary branches was modeled using relatively low elongation rates, plus growth functions which suppress the relative growth of older branches, for branches of order ≥ 2 (Table S1). Three-dimensionally preserved specimens indicate the presence of a small, spherical, basal holdfast (32).

Fig. S3. *Bradgatia linfordensis*. (A). Image reproduced with permission from Flude & Narbonne (32) Fig. 4A. (B). Image reproduced with permission from Flude & Narbonne (32) Fig. 4E. © Canadian Science Publishing or its licensors. (C) British Geological Survey cast (specimen number GSM 105873) from the Bradgate Formation, Leicestershire, UK, held in the Sedgwick Museum of Earth Sciences, Cambridge. Scale bars 1cm. (D) L-system model. Frontal view. (E) Rotated (apical) view.

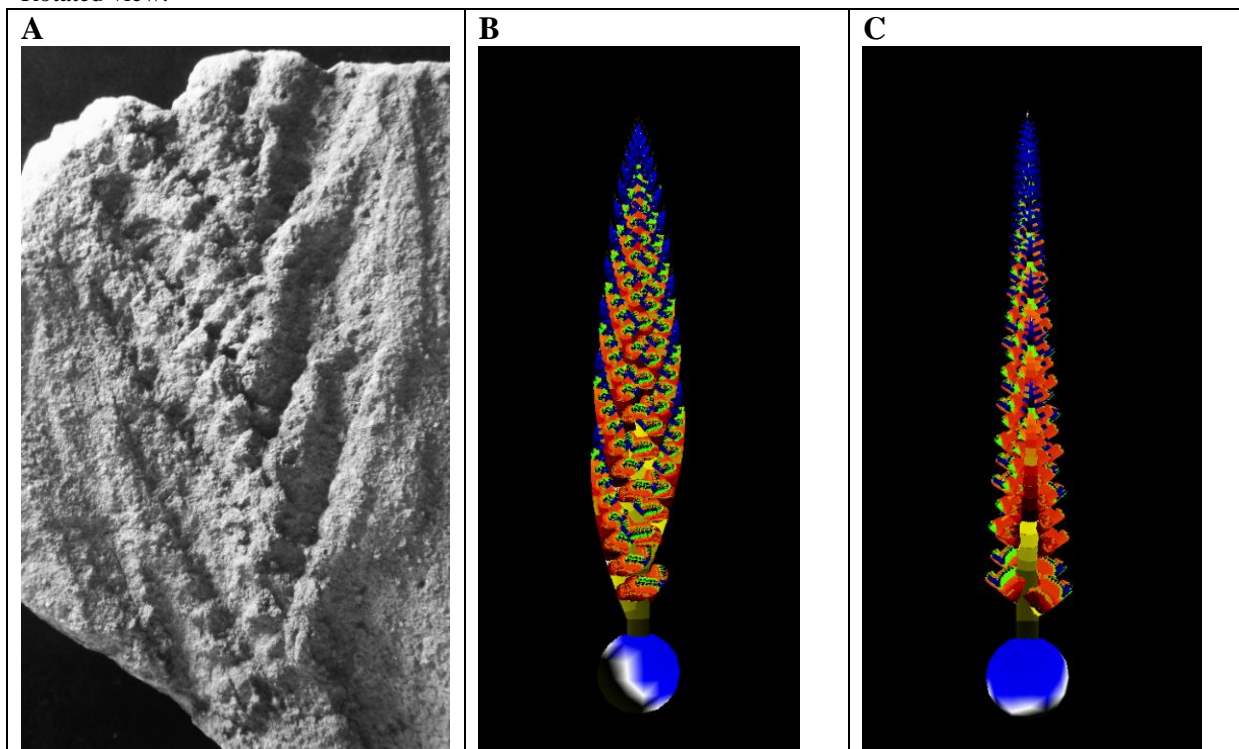


Charnia masoni

This species has regular, tightly packed alternating branches, emanating from an inferred central stem (21). Many specimens do not preserve branching structure beyond the primary branches. However, some exceptionally preserved specimens show self-similar, rangeomorph branching to 4 orders (e.g. (47) Fig. 2B). Secondary branches are visible only on one side of each primary branch in frontal view (4, 45). This is interpreted as the result of rotation of branches in an alternating series (4, 45). The close packing of primary branches makes it difficult to determine the origin and orientation of the 2nd order branches in many

specimens. However, a number of features suggest growth of 2nd order branches upwards from the primary branch (with 2nd order branch apices oriented towards the top of the frond). First, this is compatible with the widely noted zig-zag midline (e.g. Fig. S4A) here interpreted to result from stacking of the primary branches, so that the base of each 1st order branch (with its associated sub-branches) crosses over the stem and the lower part of the primary branch immediately above it. Second, this is supported by the fine-scale structure of exceptionally preserved specimens, such as that shown in Fig. S4A. In this specimen the free apices of the 2nd order branches appear to overlap upwards onto the branches above. In the lower part of this specimen, visible 3rd order branches also appear to be oriented apex-up. This branching architecture was modeled using a 270° z-axis rotation for the primary branches with 26° y-angle branching (mean of 5 measurements taken from Fig. S4A) and a 1.5° x-axis rotation giving the slight concave upper curvature. 2nd order branches were then rotated 90° around the x-axis and 45° around the y-axis and ≥3rd order branches given 340° x-axis and 20° y-axis rotations (Fig. S4C). The relatively large number of branches (up to 20 have been observed (21)), relatively even branch spacing and elongate morphology (width usually 20% to 33% of height (21)) were modeled using relatively low values for the lateral branching delay and stem elongation rate (Table S1). Several specimens preserve a holdfast (e.g. see (48) Fig. 2A, with holdfast width approximately 72% maximum frond width). The holdfast has been described as ellipsoidal (48) or globular (8) and is modeled here using a sphere.

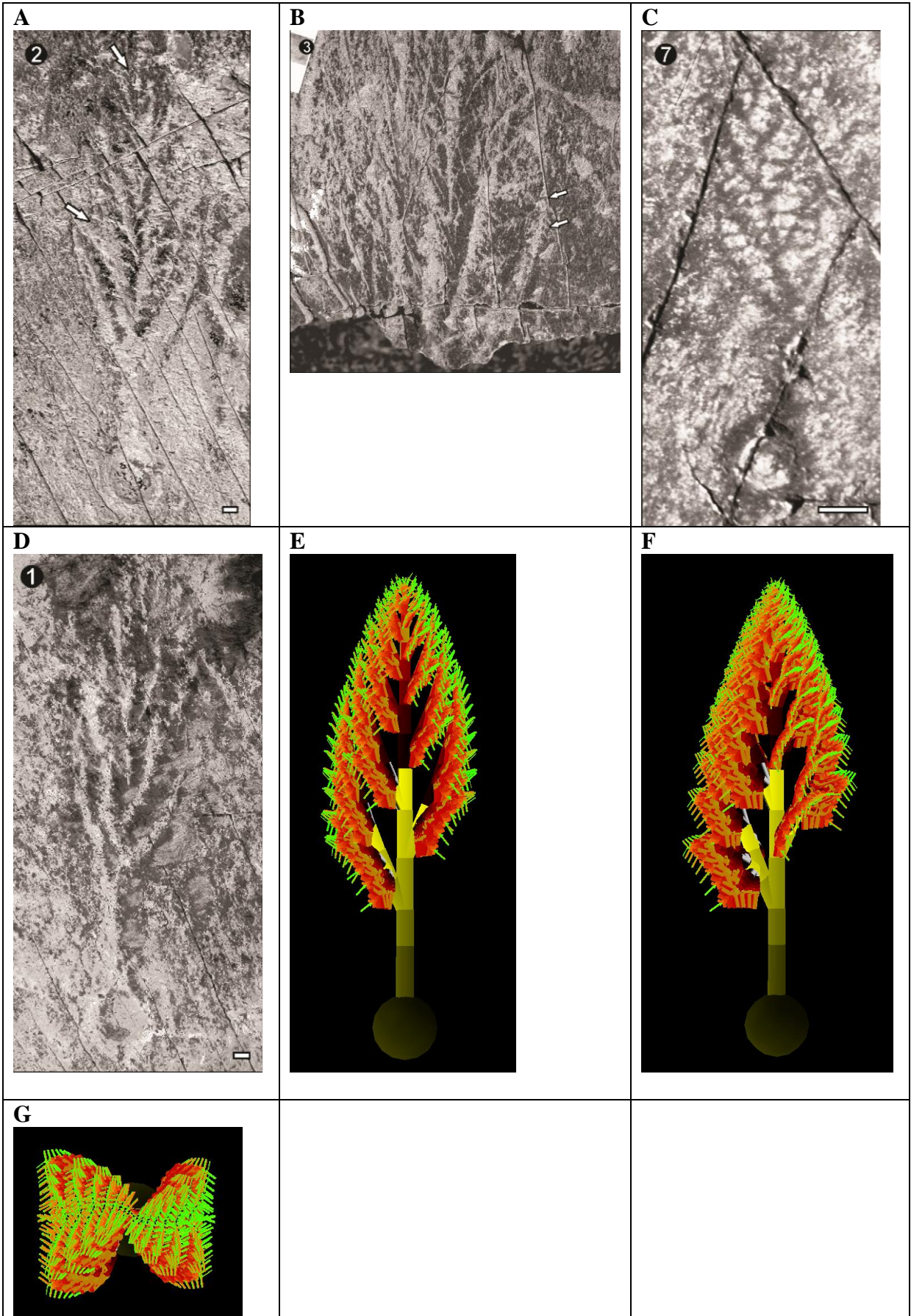
Fig. S4. *Charnia masoni*. (A) Specimen from the Rawnsley Quartzite, Flinders Ranges, South Australia. South Australia Museum specimen number P36574, described by Nedin & Jenkins (44), photograph courtesy of Jim Gehling (South Australia Museum, Adelaide, Australia). Scale bar 1cm. (B) L-system model. Frontal view. (C) Rotated view.



Culmofrons plumosa

This species is morphologically similar to *Beothukis mistakensis*, with an ovate shape (33). However, it is distinguished (33) based on a long basal stem (e.g. with basal stem height 23% of branching frond height in the holotype shown in Fig. S5A), slight zig-zag mid-line where the impression of the lateral branches obscures the inferred central stem, and the presence of approximately five alternating primary branches on either side of the central axis. The scalloped outer edge (e.g. visible to the right of Fig. S5B) suggests that secondary branches have their emergence points closer to the stem and free apices towards the extremities of the frond (as in *B. mistakensis*). Measurements were used to code y-axis angles for primary branches ($y=28^\circ$, $n=6$, Fig. S5A). A slight concave upper curvature of the primary branches was modeled using 358° x-axis curvature. Secondary branches were interpreted to have convex upper curvature (of 5°), with a sigmoidal outline (e.g. Fig. S5B) visible where secondary branches overlap (33). Secondary branches are only visible on one side of each primary branch. This could suggest that there was only a single row of secondary branches in life (33), which can be modeled using a zero or very low y-axis angle for secondary branching (e.g. see *Trepassia* as modeled below). However, the similar arrangement in *B. mistakensis* has been interpreted as a taphonomic feature, resulting from “folding” (4) or “furling” (45) of secondary branches so that one side of an alternating series is “undisplayed” (45) (as described above) and the model presented here follows this interpretation (Fig. S5E). Secondary and tertiary y-axis angles were coded based on measurements from Fig. S5B (2nd order, mean= 47° , $n=8$; 3rd order, mean= 65° , $n=6$). Figured specimens of *C. plumosa* are only moderately well preserved in comparison with the best preserved specimen of *B. mistakensis* (Fig. S2A; Narbonne et al. (4) Fig. 5.1). However, differences in the strength of the impression of branches on the left and right of the stem (e.g. Fig. S5B,D) are compatible with a small amount of helical torsion in *C. plumosa* (Fig. S5D-E), as reported for *B. mistakensis* (4). The width of the branching frond was measured at 42% of frond height, basal stem height was 23% of branching frond height, and holdfast width was 32% of frond width (holotype, Fig. S5A). As some three-dimensionality of the holdfast is preserved (e.g. Fig. S5C), this was modeled as a sphere. The long basal stem was modeled using relatively high elongation rate for the basal stem segment (Table S1). The slight zig-zag mid-line visible in the fossil specimens (e.g. Fig. S5A) is interpreted to result from the impression of the relatively densely packed alternating primary branches, which slightly overlap the mid-line (Fig. S5E-G).

Fig. S5. *Culmofrons plumosa*. (A) Image reproduced with permission from Laflamme et al. (33) Fig. 2.2. Holotype specimen. (B) Image reproduced with permission from Laflamme et al. (33) Fig. 2.3. (C) Image reproduced with permission from Laflamme et al. (33) Fig. 2.7. (D) Image reproduced with permission from Laflamme et al. (33) Fig. 2.1. Scale bars 1cm. (E) L-system model. Frontal view. (F) Rotated view. (G) Apical view.



Fractofusus andersoni* and *Fractofusus misrai

Genus *Fractofusus* contains two species: *Fractofusus andersoni* (details here) and *Fractofusus misrai* (details below), represented in Newfoundland by hundreds to thousands of specimens (15). The species share a similar fusiform (“spindle”) morphology, which has been interpreted to result from two main poles of growth, one at either end of the central axis (7). Within the L-system formalism used here, this morphology is modeled using a duplication and 180° y-axis rotation of the branching axiom, so that growth proceeds in parallel from two 0-order apices, representing the top and bottom of the stem (as oriented in the images below). The fossils preserve an external mold of the lower surface of the organism, inferred to have been in contact with the sediment in life due to the unusually good preservation of many specimens and the lack of a visible holdfast (15). Three-dimensional curvature of these impressions indicates that each primary branch and its associated higher order branches had a convex outer curvature, modeled here using x-axis curvature of branches of order ≥ 1 (Table S1). Interestingly, folded specimens of *F. misrai* (see Fig. S7A) indicate a similar convex outer curvature for both the upper and lower sides of the organism (15). This morphology is modeled here using rotations of growth axes for the primary branches (90° z-axis rotation around the stem plus primary branch rotations of 90° around the x-axis, 90° around the y-axis and 270° around the z-axis). This gives convex outer curvature to the primary branches on both upper and lower surfaces (as oriented in Fig. S6C and Fig. S7C) and orients the primary branches perpendicular to the long axis (90°, mean of 13 measurements taken from Gehling & Narbonne (15) Fig.8C). Y-axis branching angles for branches of order ≥ 2 were modeled at 24° for *F. misrai* (mean of 8 secondary branching angle measurements from (15) Fig.8C) and 38° for *F. andersoni* (mean of 14 secondary branching angle measurements from (15) Fig.12C).

The two *Fractofusus* species are distinguished by the greater number of visible primary branches and more elongate morphology of *F. misrai* (with approximately 20 primary branches and width around 30% of length) compared with *F. andersoni* (with approximately 10 primary branches and width around 65% of length) (15).

Fig. S6. *Fractofusus andersoni*. (A) Image reproduced with permission from Gehling & Narbonne (15) Fig.12C. Scale bar 1cm. © Canadian Science Publishing or its licensors. (B) L-system model. Frontal view. (C) Rotated (apical) view.

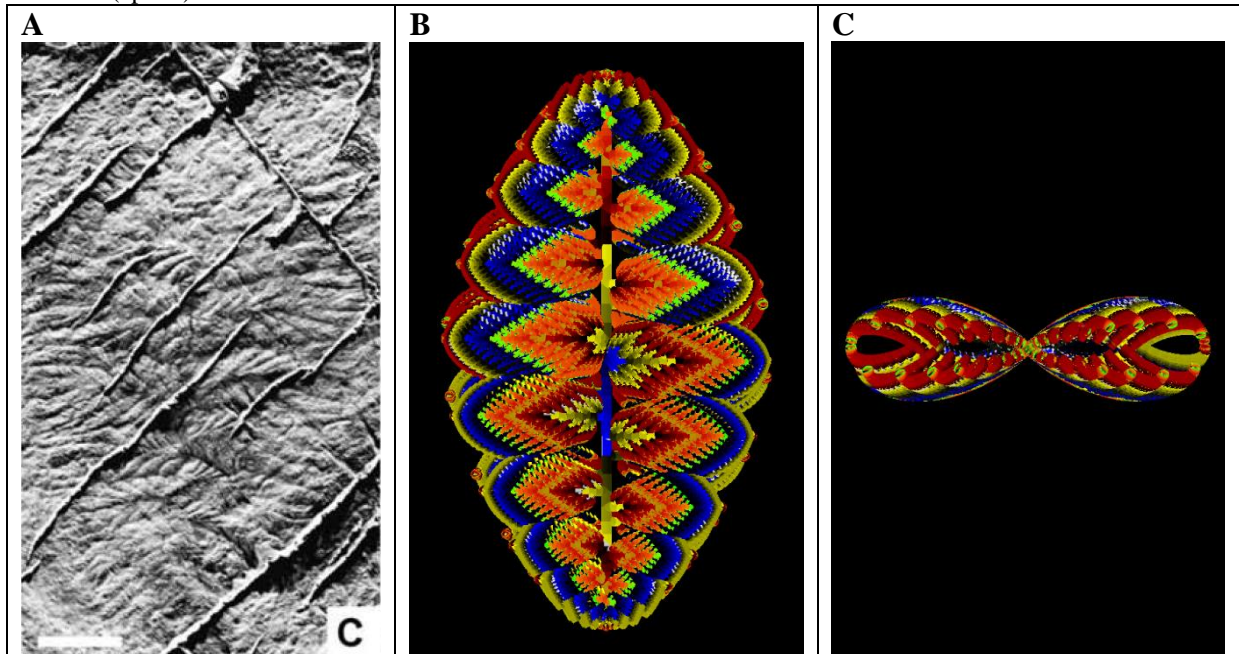
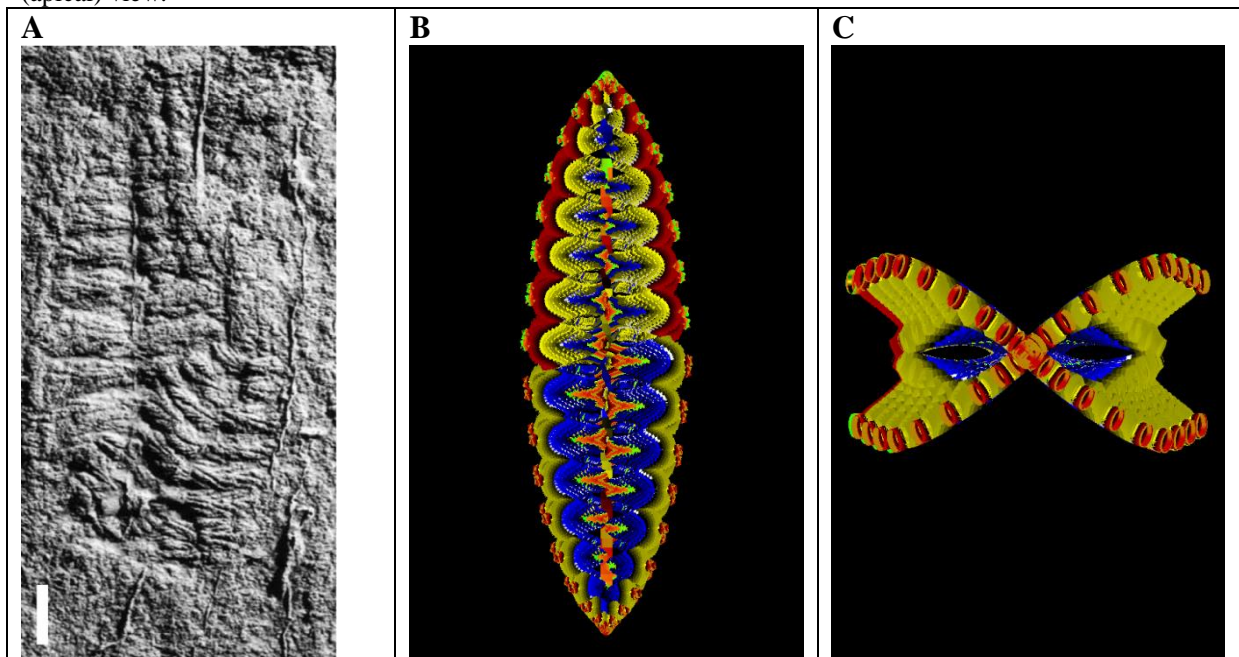


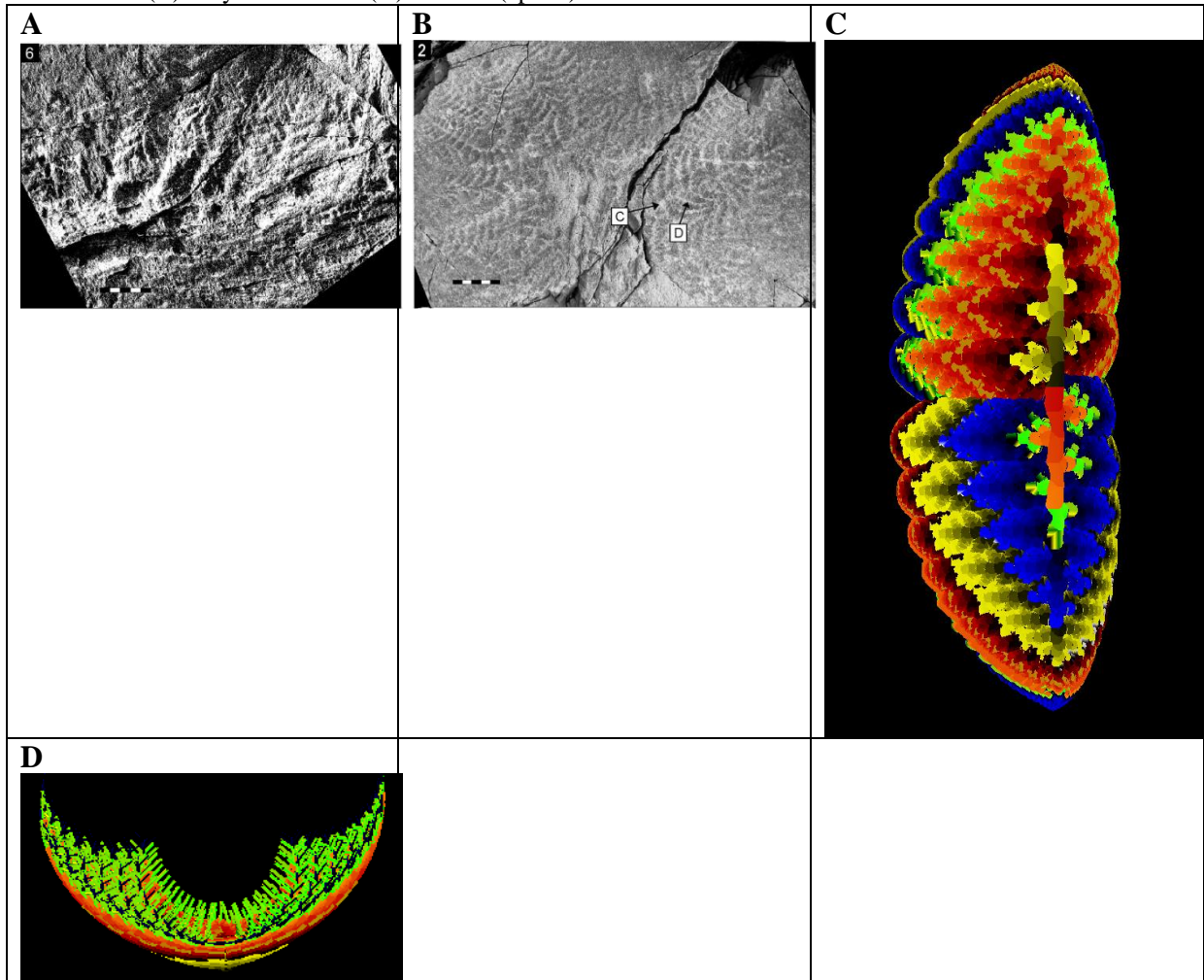
Fig. S7. *Fractofusus misrai*. (A) Image reproduced with permission from Gehling & Narbonne (15) Fig.8C. Scale bar 1cm. © Canadian Science Publishing or its licensors. (B) L-system model. Frontal view. (C) Rotated (apical) view.



Hapsidophyllas flexibilis

Multiple specimens of this taxon have been reported from Mistaken Point, Newfoundland (49). However, preservation is relatively poor. Large lateral branches appear to emerge from a thick central axis (Fig. S8A) and no holdfast is preserved, suggesting that *H. flexibilis* was a benthic recliner, morphologically similar to *Pectinifrons abyssalis* (see model below) (49). Unlike *P. abyssalis*, however, specimens of *H. flexibilis* show impressions of lateral branches on both sides of the inferred central axis (e.g. Fig. S8B), although the relative preservation of the two sides varies between specimens (49). The smallest lateral branches lie at either end of the central axis (e.g. Bamforth & Narbonne (49) Fig. 5; Fig. S8A), compatible with two main growth axes as suggested for *Fractofusus* (7) and *Pectinifrons* (although lateral branches are of relatively similar lengths throughout). The strength of the impression left by a lateral branch can be seen to decrease progressively towards its apex (Fig. S8A) (49), suggesting concave upper curvature of the primary branches (Table S1). In specimen Fig. S8B the total height of the organism is approximately 66% of width (as oriented in Fig. S8B). These features are here interpreted to indicate a reclining life position, with the central axis in contact with the sediment and two alternating rows of lateral branches curving upwards along their length, into the water column, which were felled to the seabed prior to fossilization (49). Unlike the benthic recliner *Fractofusus* (15), no longitudinally folded specimens have been reported to suggest a double-layered structure. The angle of the large lateral branches (1st order in the L-system numbering used here) from the central axis is variable, and it has been suggested that these were flexible in life (49). The mean of six measurements from the partial specimen shown in Fig. S8A was used to code a y-axis branch growth angle of 88°. Eight measurements for the 2nd order branches gave a y-axis mean of 52°.

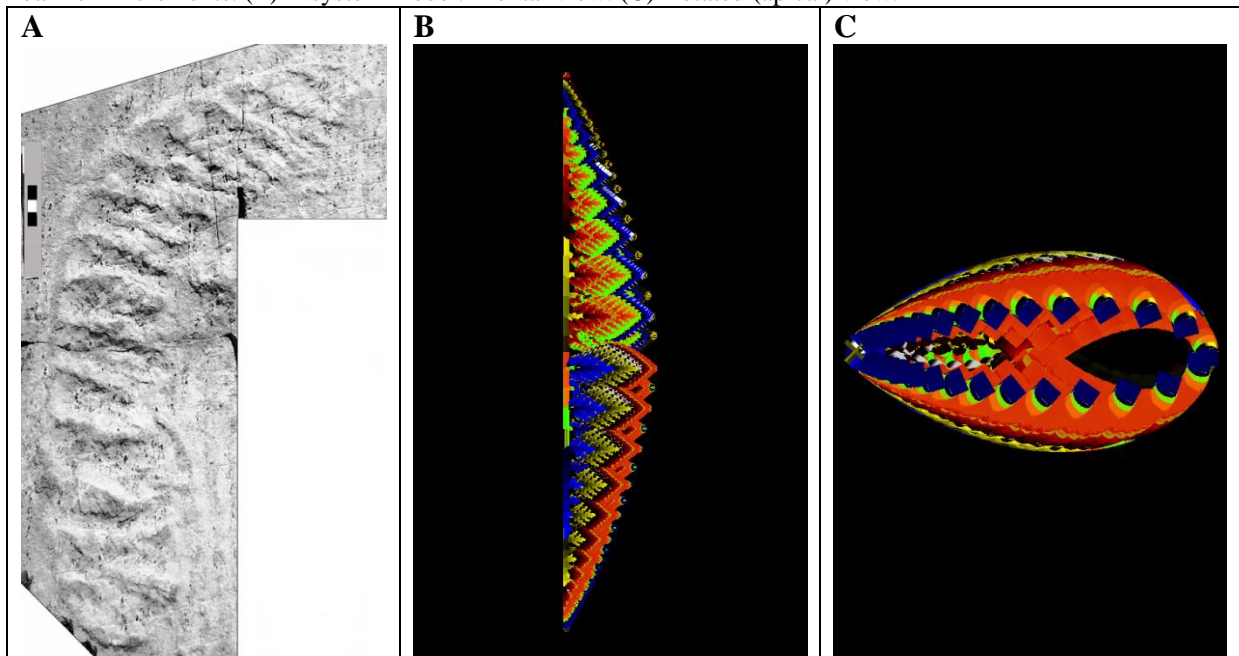
Fig. S8. *Hapsidophyllas flexibilis*. (A) Image reproduced with permission from Bamforth & Narbonne (49) Fig. 5.6. (B) Image reproduced with permission from Bamforth & Narbonne (49) Fig. 4.2. Scale bars 1cm increments. (C) L-system model. (D) Rotated (apical) view.



Pectinifrons abyssalis

This species, known from a number of Newfoundland specimens, has a distinctive pectinate (comb-shaped) morphology (Bamforth et al. (50)), with two rows of alternating branches. In the fossil specimens one of these rows overlies the other, so that both are preserved on the same side of the stem (Fig. S9A). These primary branches lie approximately perpendicular to the stem in the fossil specimens (50). This morphology was modeled using three rotations for the primary branches (x-axis 90° , y-axis 45° , z-axis 270°). Curvature of the stem is visible in some specimens (e.g. Fig. S9A). A C-shaped curve of the stem has been interpreted as a possible biological feature (50). However, fossil specimens show variable stem curvature (e.g. see S-shaped specimen illustrated in (50) Fig. 7). Therefore, this is interpreted here as taphonomic variability and the stem is modeled as uncurved in the life position (Fig. S9B). Branching structure for order 2 is poorly preserved however this is visibly acute (and was modeled here using an approximate y-axis branching angle of 38°).

Fig. S9. *Pectinifrons abyssalis*. (A) Image reproduced with permission from Bamforth et al. (50) Fig. 4.1. Scale bar 1cm increments. (B) L-system model. Frontal view. (C) Rotated (apical) view.

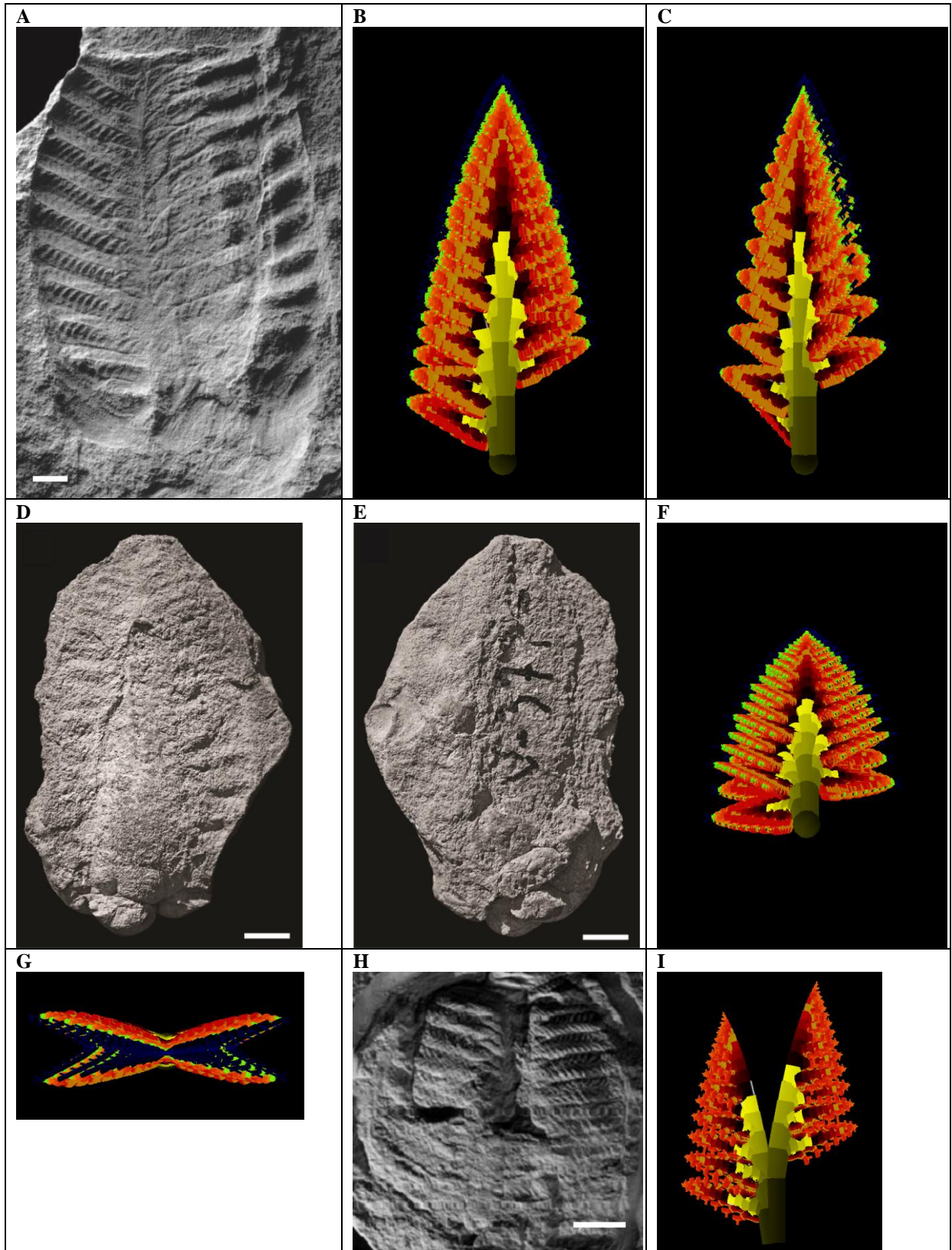


Rangea schneiderhoehni

In this species, the alternating branches are thought to be arranged into >2 vanes or rows (51). Interpretations of the number of vanes differ, at three (51), four (52) and five to six (35). Here, the multi-vane arrangement is interpreted to result from a low y-axis angle of 8° for primary branching, combined with z-axis rotations (of 202.5° and 135° , respectively, for the primary and secondary branches). These rotations orient the secondary branches into four vertical rows, compatible with previous suggestions of four “vanes” (Fig. S10G), which form a tetradial arrangement when viewed from above (52). In long-axis rotations (e.g. Fig. S10C), only three of these rows are clearly visible. This arrangement is compatible with previous observations of up to three vanes in flattened fossil specimens (e.g. Fig. S10A), where a third vane may be visible when only partially overlapped by the vane above it (51). New specimens confirm the presence of a central stem (“axial stalk”) and “axial bulb” (35), interpreted here as a small holdfast. Holdfast width was estimated at approximately 18% of maximum frond width from Vickers-Rich et al. (35) Fig. 6.1. Vickers-Rich et al. (35) suggested that new three-dimensional specimens from southern Namibia preserve five to six

vanes. However, the model presented here is similar in basal view to their figured specimen (compare Fig. S10E-F). The grouping of secondary and higher branches on primary branches that lie very close to the stem is consistent with partial specimens that reveal branch positions (compare partial fossil specimen Fig. S10H and a partial model in which only the basal primary branches are displayed Fig. S10I). The relatively compact body form was modeled using low to moderate values for lateral branching delays and elongation rates (Table S1).

Fig. S10. *Rangea schneiderhoehni*. (A) Specimen from the Kliphoek Member, Dabis Formation, Namibia. Image reproduced with permission from Grazhdankin & Seilacher (51) Fig. 2. Scale bar 1cm. (B) L-system model. Frontal view. (C) Rotated view. (D) Image reproduced with permission from Vickers Rich et al. (35) Fig. 8.1. Specimen NESM F635-c lower view. (E) Image reproduced with permission from Vickers Rich et al. (35) Fig. 8.2. Specimen NESM F635-c upper view. Scale bars 1cm. (F) L-system model. View from below. (G) View from above. (H) Partial specimen. Image reproduced with permission from Grazhdankin & Seilacher (51) Fig.7. Scale bar 1cm. (I) Partial model illustrating the relative positions of two sequential lateral branches.



Trepassia wardae

Initially described as *Charnia wardi* (1) and redefined as *Trepassia wardae* (4), this is an elongate species, with a width to height ratio of 1.6:6 cm (width 26% height) measured from an exceptionally preserved 3-D specimen from Spaniard's Bay (4). Specimens from the Drook Formation, preserved as flattened impressions, are the longest known Ediacaran fronds, up to 1.85 m in height (with width <10% of height (1)). Previous interpretations have suggested that the primary and secondary branches originate close to the main stem, to which they may both have been attached (4). As a result, most primary and secondary branch origins are concealed. However, a measurement for the lowest primary branch, visible in Narbonne et al. (4) Fig. 10.4 (Fig. S11D) gave a y-axis branching angle of 4°. An x-axis curvature of 7° for the 2nd order branches was used to model their convex upper curvature. Here, primary and secondary branches are interpreted to emerge at an acute angle so that both lie close to the main body axis. The branches acute to perpendicular to the stem (mean=82°, n=6) are then interpreted to be 3rd order (rather than 2nd order as previously suggested by Narbonne et al. (4)). This branching pattern is compatible with both details of fossil morphology (compare details Fig. S11D and Fig. S11E below) and the elongate overall morphology of the frond, which is increased by the near-vertical orientation of the 1st and 2nd order branches. Only one side of the 1st and 2nd order branches is visible in front or back view (4). This is interpreted as the result of a z-axis rotation of 90° for the 1st order branches. This model used a moderate lateral branching delay and a moderate increase in elongation rate relative to the stem for branches of order ≥ 2 (Table S1). Holdfast width was estimated at approximately 47% of frond width, from Narbonne et al. (4) Fig. 10.4.

Fig. S11. *Trepassia wardae*. (A) Specimen from Spaniard's Bay, Newfoundland. Image reproduced with permission from Narbonne et al. (4) Fig. 10.1. Scale bar 1cm. (B) L-system model. Frontal view. (C) Rotated view. (D) Detail of Narbonne et al. (4) Fig. 10.4. Scale bar 1cm. (E) Detail from L-system model.

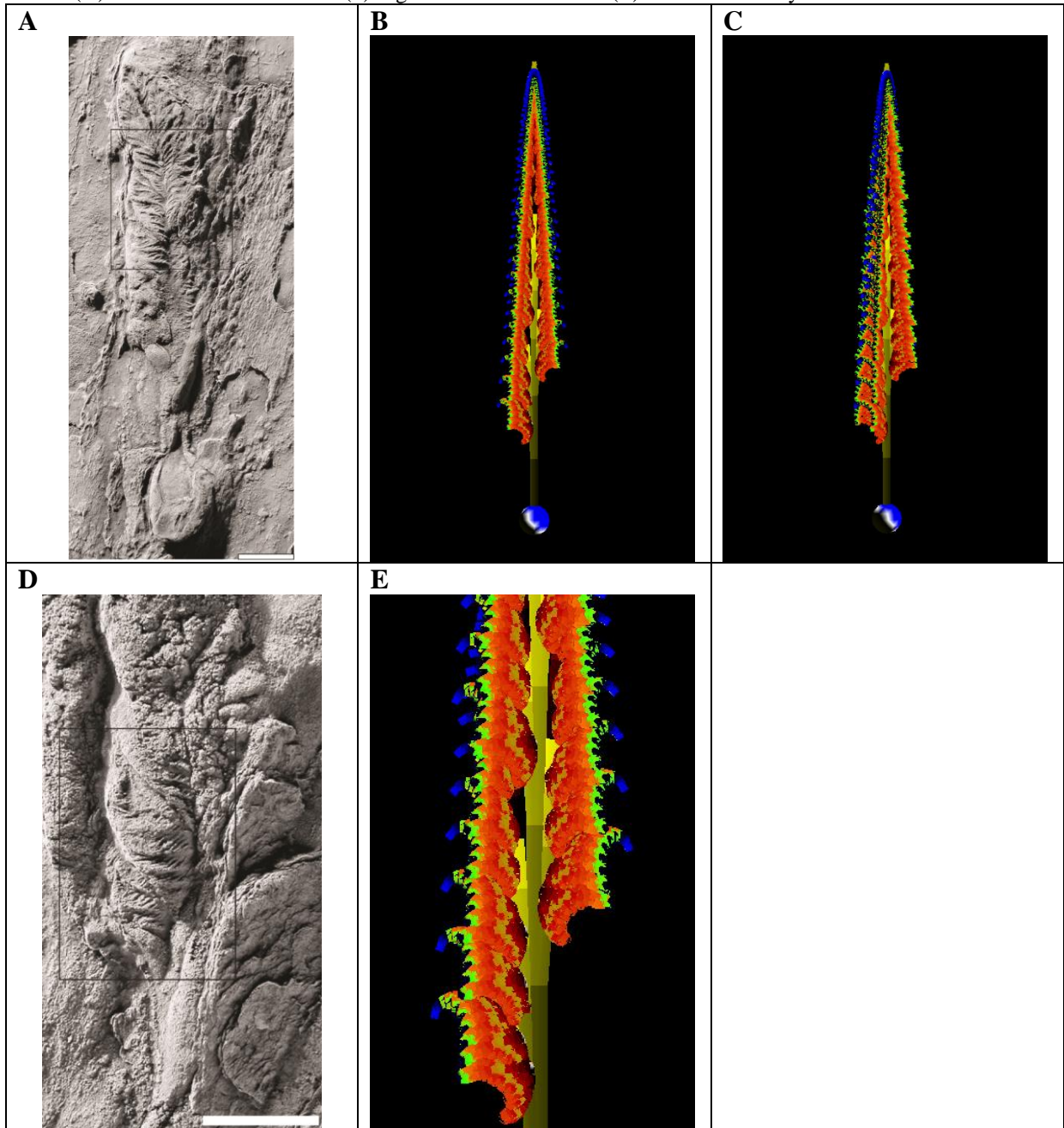


Fig. S12. Dendrogram showing hierarchical clustering of modeled rangeomorph dimensions (see Table S2 for values). Species labels: 1. *Avalofractus abaculus* 2. *Beothukis mistakensis* 3. *Bradgatia linfordensis* 4. *Charnia masoni* 5. *Culmofrons plumosa* 6. *Fractofusus andersoni* 7. *Fractofusus misrai* 8. *Hapsidophyllas flexibilis* 9. *Pectinifrons abyssalis* 10. *Rangea schneiderhoehni* 11. *Trepassia wardae*.

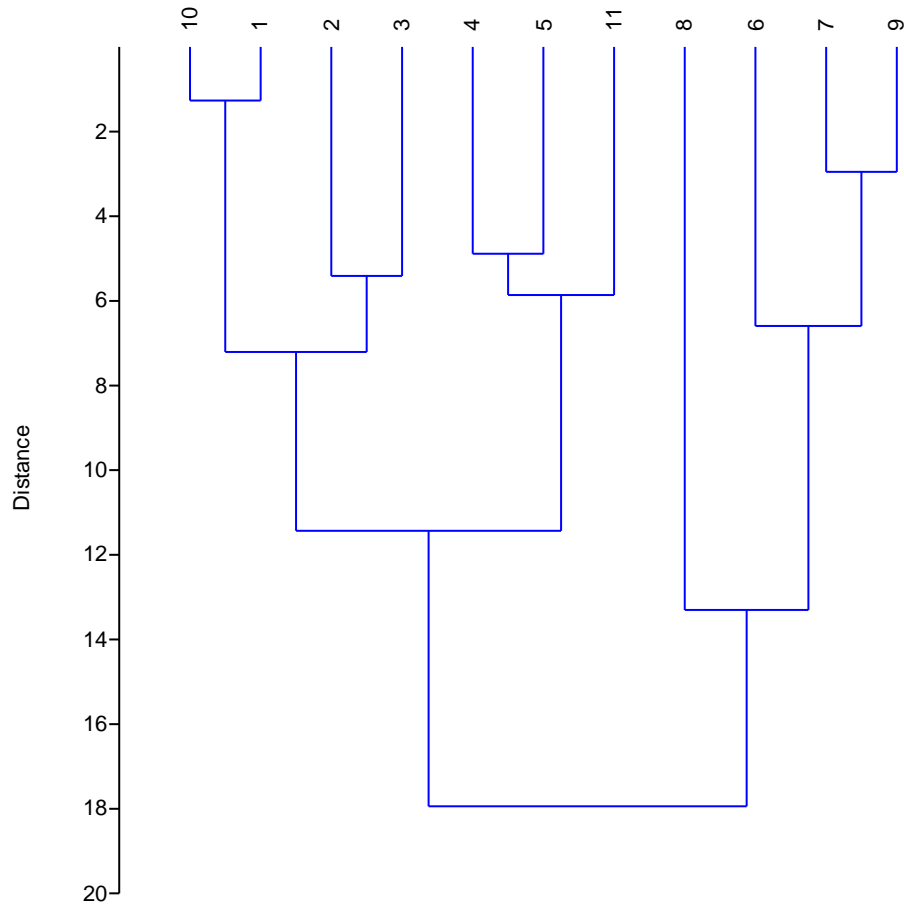
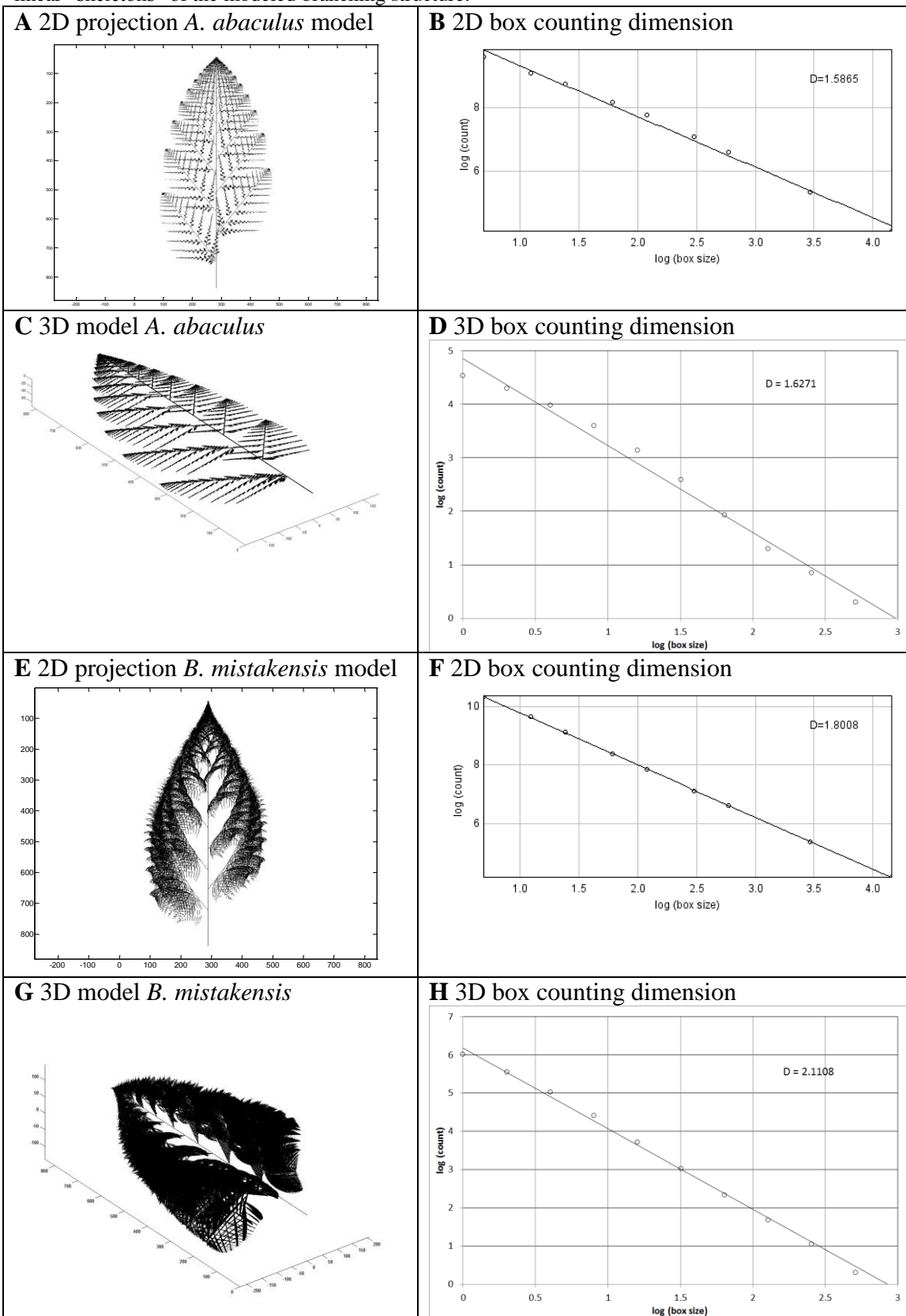
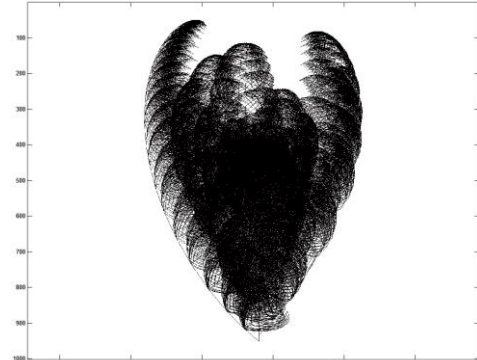


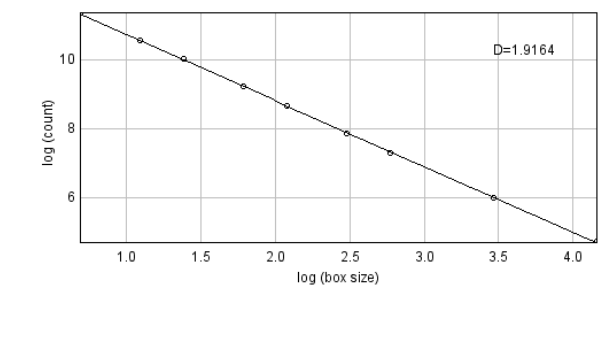
Fig. S13. Fractal dimensions. Box counting estimates of the fractal dimension in 2D and 3D. Input images are linear “skeletons” of the modeled branching structure.



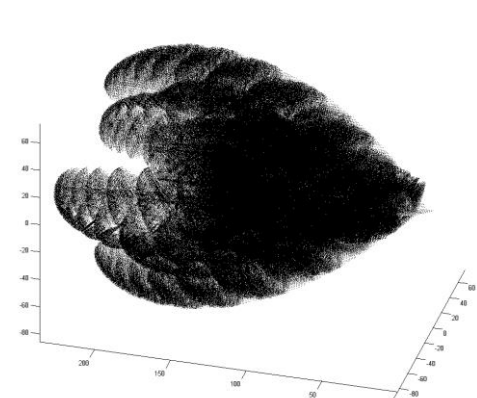
I 2D projection *B. linfordensis* model



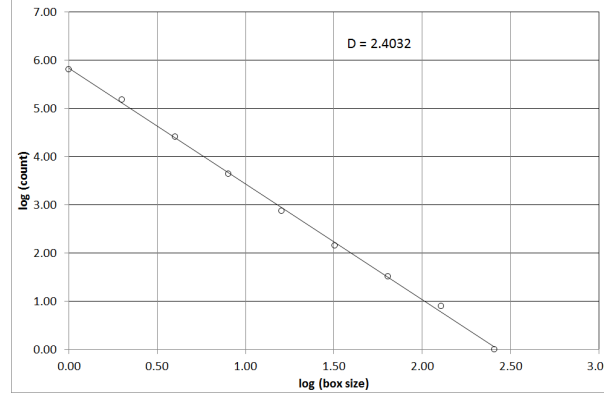
J 2D box counting dimension



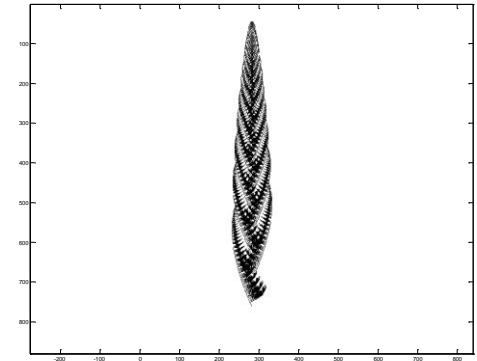
K 3D model *B. linfordensis*



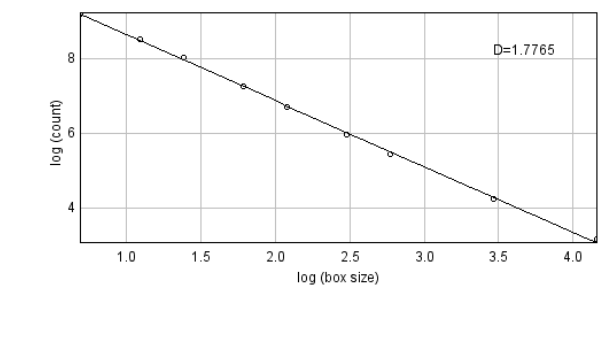
L 3D box counting dimension



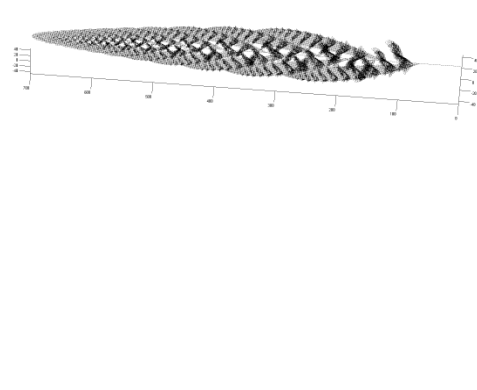
M 2D projection *C. masoni* model



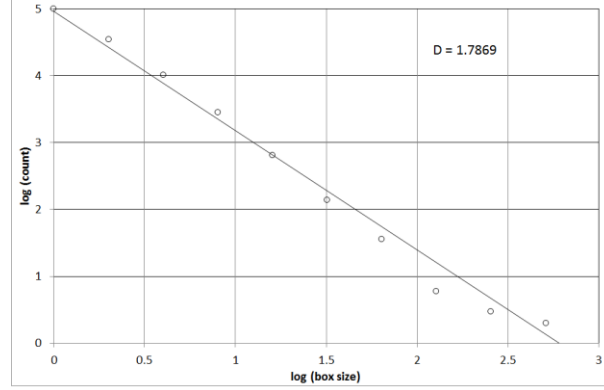
N 2D box counting dimension



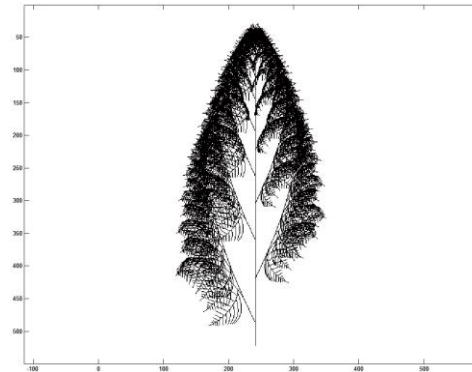
O 3D model *C. masoni*



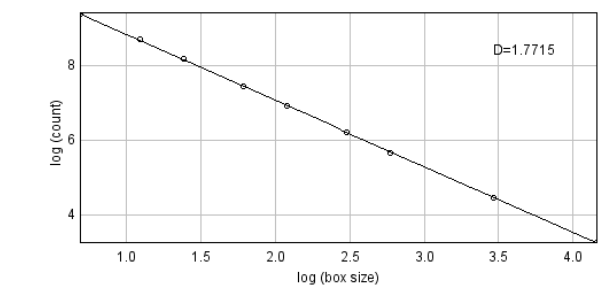
P 3D box counting dimension



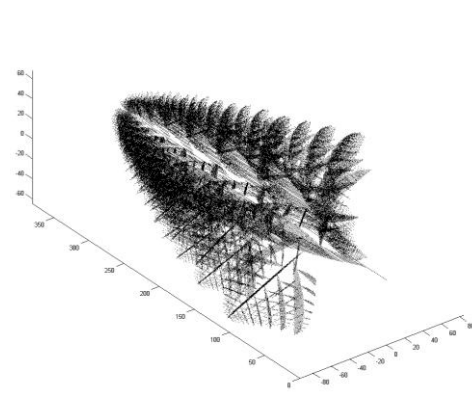
Q 2D projection *C. plumosa* model



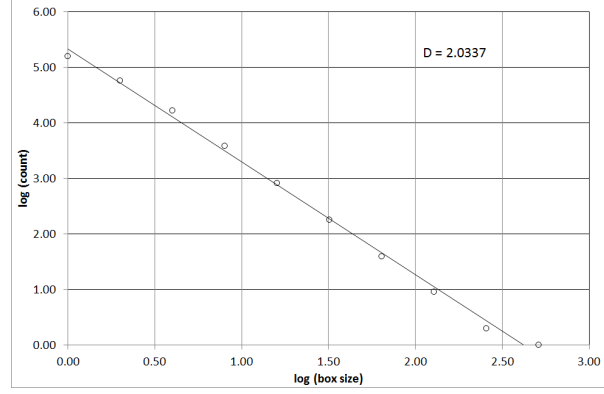
R 2D box counting dimension



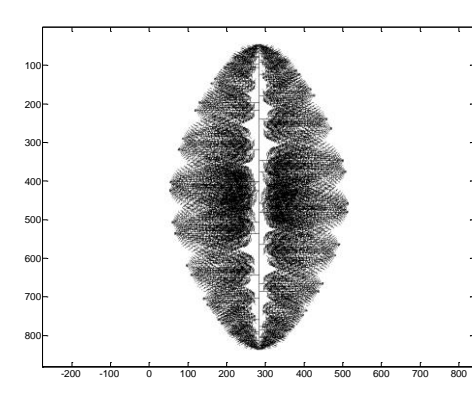
S 3D model *C. plumosa*



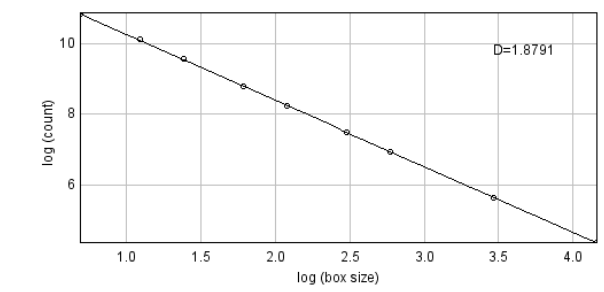
T 3D box counting dimension



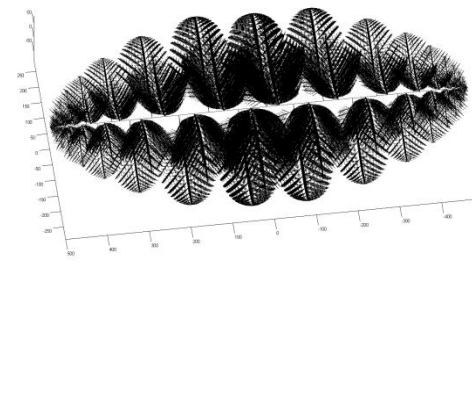
U 2D projection *F. andersoni* model



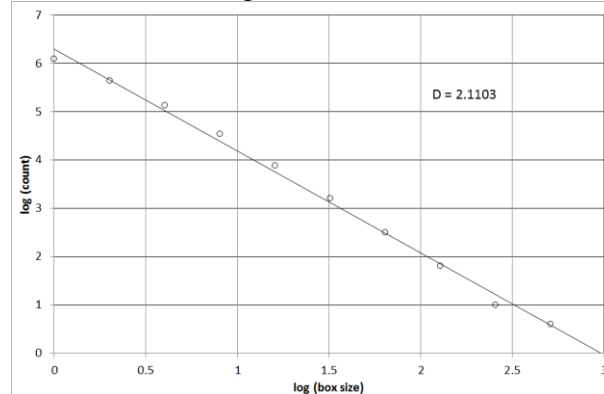
V 2D box counting dimension



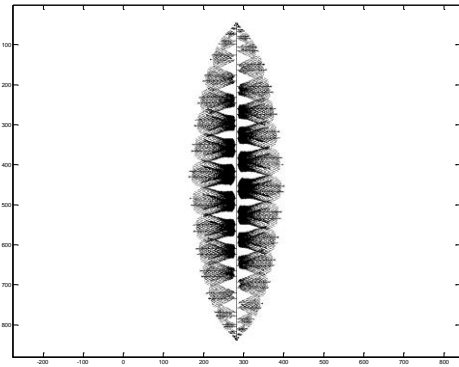
W 3D model *F. andersoni*



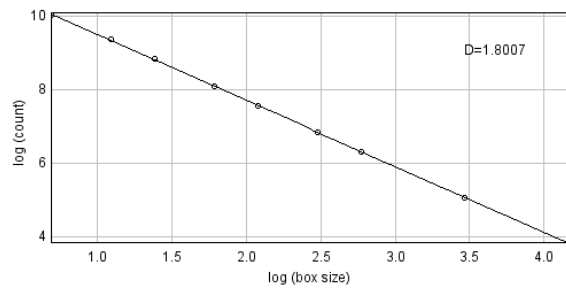
X 3D box counting dimension



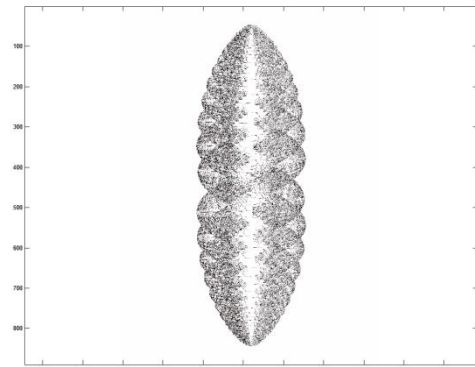
Y 2D projection *F. misrai* model



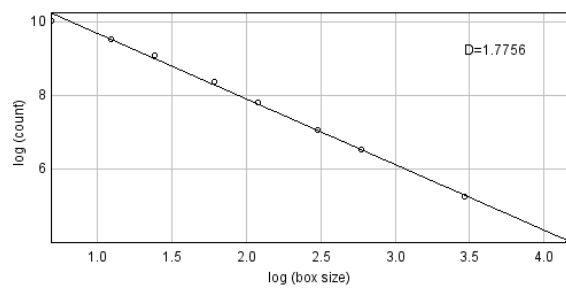
Z 2D box counting dimension



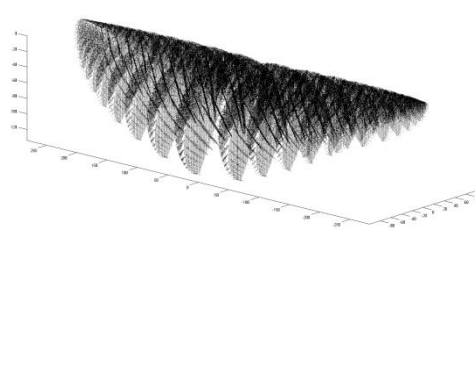
AA 2D projection *H. flexibilis* model



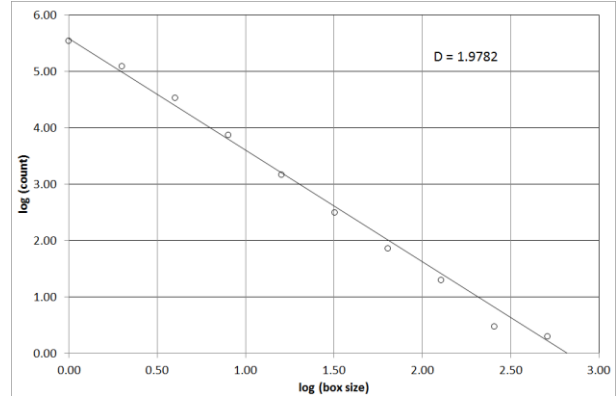
AB 2D box counting dimension



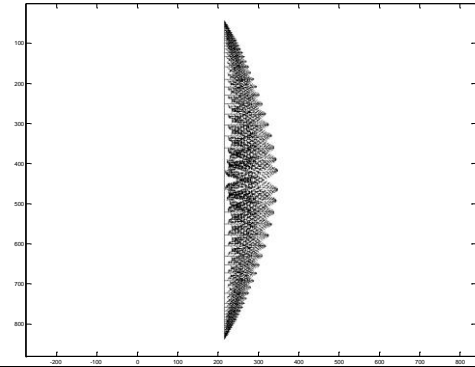
AC 3D model *H. flexibilis*



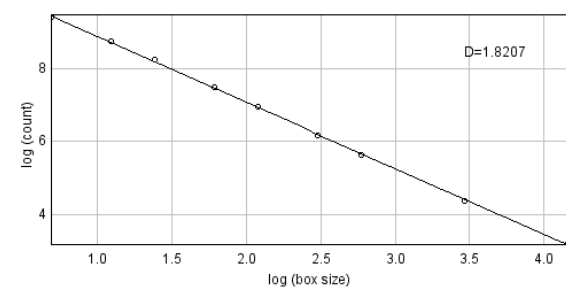
AD 3D box counting dimension



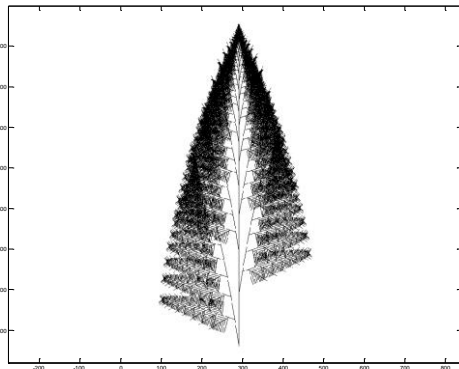
AE 2D projection *P. abyssalis* model



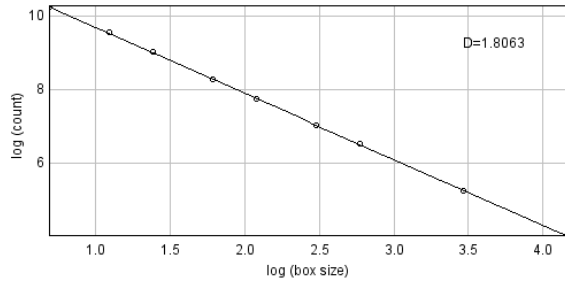
AF 2D box counting dimension



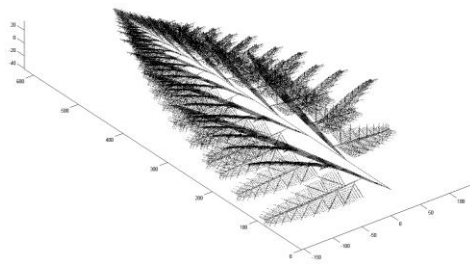
AG 2D projection *R. schneiderhoehni* model



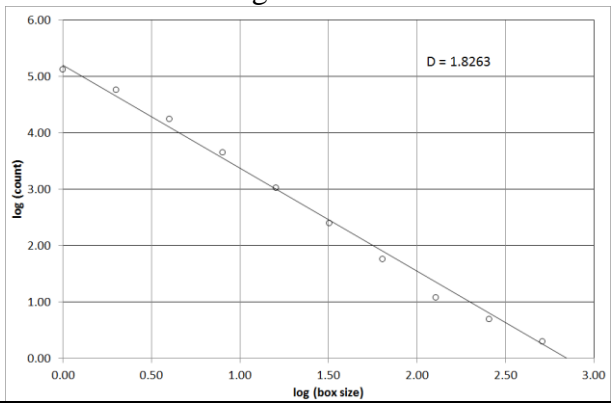
AH 2D box counting dimension



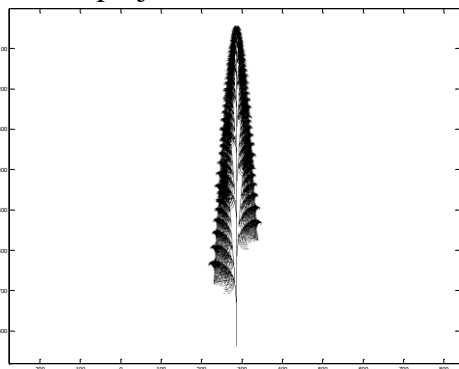
AI 3D model *R. schneiderhoehni*



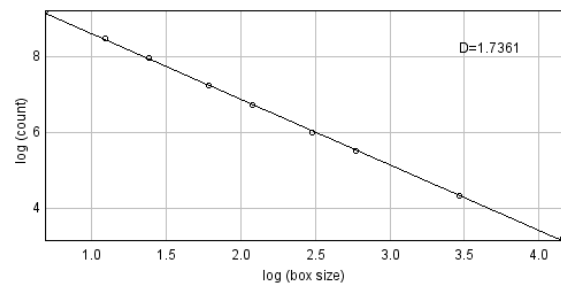
AJ 3D box counting dimension



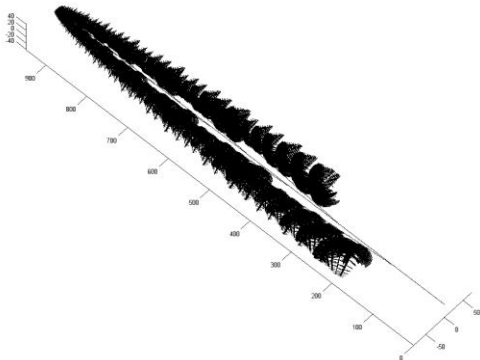
AK 2D projection *T. wardae* model



AL 2D box counting dimension



AM 3D model *T. wardae*



AN 3D box counting dimension

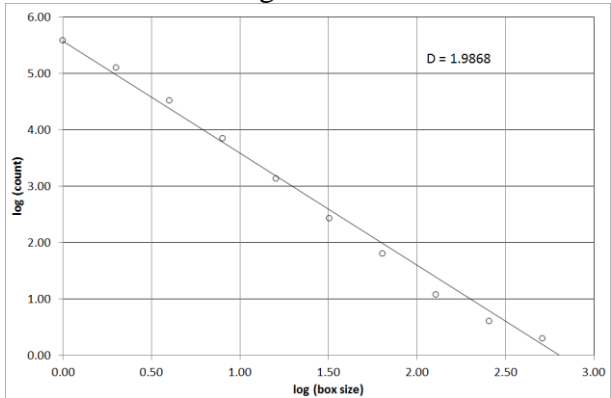


Table S1. L-system parameters

Species	Parameter	Holdfast diameter (L-system world units)	Elongation rate			
	Branch order		0	1	2	≥3
<i>Avalofractus abaculus</i>		60	1.115	1.125	1.125	1.125
<i>Beothukis mistakensis</i>		80	1.115	1.120	1.130	1.130
<i>Bradgatia linfordensis</i>		5	1.06	1.114	1.07	1.07
<i>Charnia masoni</i>		50	1.100	1.085	1.050	1.050
<i>Culmofrons plumosa</i>		30	1.115	1.114	1.13	1.13
<i>Fractofusus andersoni</i>		N	1.100	1.100	1.125	1.125
<i>Fractofusus misrai</i>		N	1.110	1.080	1.120	1.120
<i>Hapsidophyllas flexibilis</i>		N	1.1	1.1	1.11	1.1
<i>Pectinifrons abyssalis</i>		N	1.115	1.125	1.125	1.125
<i>Rangea schneiderhoehni</i>		20	1.115	1.110	1.110	1.050
<i>Trepassia wardae</i>		30	1.115	1.115	1.130	1.130

Elongation rate Basal stem segment	Branching delay (prop. iterations)				x curvature angle (°) 0	y zig-zag angle (°) 0
	0	1	2	≥3		
1.125	0.00	0.21	0.21	0.24	0.0	0.0
1.040	0.00	0.24	0.16	0.16	0.0	0.0
N	0.00	0.21	0.08	0.08	0.0	0.0
N	0.00	0.13	0.18	0.21	0.0	0.0
1.1	0.00	0.29	0.21	0.16	0.0	0.0
N	0.00	0.16	0.24	0.24	0.0	0.0
N	0.00	0.00	0.22	0.11	0.0	0.0
N	0.00	0.00	0.26	0.29	0.0	0.0
N	0.00	0.20	0.20	0.23	0.0	0.0
N	0.00	0.24	0.16	0.18	0.0	0.0
N	0.00	0.24	0.16	0.16	0.0	0.0

z torsion angle (°) 0	x curvature angle (°) 1	y zig-zag angle (°) 1	z rotation angle (°) 1	x curvature angle (°) ≥2
0.0	0.0	0.0	0.0	0.0
355.0	357.0	0.0	0.0	5.0
42.5	355.0	0.0	0.0	355.0
0.0	1.5	0.0	0.0	359.5
357.0	358.0	0.0	0.0	5.0
90.0	4.0	0.0	0.0	4.0
90.0	1.0	0.0	0.0	2.0
0.0	5.0	0.0	0.0	5.0
0.0	4.0	0.0	0.0	4.0
0.0	358.0	0.0	135.0	359.0
0.0	0.0	0.0	0.0	7.0

y zig-zag angle (°) ≥2	z rotation angle (°) ≥2	x branching angle (°) 1	y branching angle (°) 1	z branching angle (°) 1
0.0	0.0	15.0	38.0	0.0
0.0	0.0	0.0	43.0	90.0
0.0	0.0	0.0	55.0	90.0
0.0	0.0	0.0	26.0	270.0
0.0	0.0	0.0	28.0	90.0
0.0	0.0	90.0	90.0	270.0
0.0	0.0	90.0	90.0	270.0
0.0	0.0	0.0	88.0	0.0
0.0	0.0	90.0	45.0	270.0
0.0	0.0	0.0	8.0	202.5
0.0	0.0	0.0	4.0	90.0

x branching angle (°) 2	y branching angle (°) 2	z branching angle (°) 2	x branching angle (°) ≥3
15.0	47.0	0.0	15.0
0.0	46.0	0.0	0.0
0.0	45.0	0.0	355.0
90.0	45.0	0.0	340.0
0.0	47.0	0.0	0.0
0.0	38.0	0.0	0.0
0.0	24.0	0.0	0.0
0.0	52.0	0.0	0.0
0.0	38.0	0.0	0.0
0.0	64.0	345.0	0.0
0.0	0.0	0.0	0.0

y branching angle (°) ≥3	z branching angle (°) ≥3
47.0	0.0
56.0	0.0
0.0	0.0
20.0	0.0
65.0	0.0
38.0	0.0
24.0	0.0
52.0	0.0
38.0	0.0
45.0	0.0
82.0	0.0

Table S2. Estimated functional properties

Species	Length fossil (cm)	Source of length estimate	Estimated width (cm)
<i>Avalofractus abaculus</i>	9.4	Holotype measurement from Narbonne et al 2009	3.2
<i>Beothukis mistakensis</i>	14.0	Mean from Brasier and Antcliffe 2009	5.7
<i>Bradgatia linfordensis</i>	12.2	Mean from Flude & Narbonne 2008	8.1
<i>Charnia masoni</i>	20.0	Upper limit in classification of Laflamme et al 2007	2.7
<i>Culmofrons plumosa</i>	20.3	Mean from Laflamme et al 2012	7.0
<i>Fractofusus andersoni</i>	7.3	Range median from Gehling & Narbonne 2007	7.3
<i>Fractofusus misrai</i>	12.5	Range median from Gehling & Narbonne 2007	12.5
<i>Hapsidophyllas flexibilis</i>	23.2	Mean from Bamforth & Narbonne 2009	23.2
<i>Pectinifrons abyssalis</i>	15.0	Mean from Bamforth et al 2008	15.0
<i>Rangea schneiderhoehni</i>	9.0	Estimate from Fig 8 of Vickers-Rich et al 2013	4.4
<i>Trepassia wardae</i>	25.0	Mean from Laflamme et al 2007 and Narbonne et al 2009	3.6
mean	15.3		8.4
variance	36.2		38.9

Tissue thickness (mm)				0
Estimated height (cm)	Estimated depth (cm)	Bounding volume (cm ³)	Relative bounding volume (longest axis scaled to 1)	Total SA (cm ²)
9.4	1.1	34.0	0.04	77.1
14.0	3.5	279.0	0.10	455.6
12.2	8.0	796.8	0.44	1591.0
20.0	2.7	143.2	0.02	1067.7
20.3	5.0	712.8	0.09	1332.3
1.1	4.2	33.7	0.09	486.6
1.9	3.8	89.5	0.05	1599.8
5.5	8.1	1037.3	0.08	5787.8
1.2	2.4	42.4	0.01	221.1
9.0	1.1	42.9	0.06	218.0
25.0	1.9	175.8	0.01	1159.6
10.9	3.8	307.9	0.09	1272.4
68.7	6.0	131910.1	0.01	2558640.6

0.1	0.5	1	0.1	0.5	1
Tissue volume (cm³)	Tissue volume (cm³)	Tissue volume (cm³)	SA/V (cm²/cm³)	SA/V (cm²/cm³)	SA/V (cm²/cm³)
0.8	5.8	15.6	92.1	13.3	4.9
1.3	7.0	15.3	352.4	65.2	29.8
12.5	94.2	289.4	127.0	16.9	5.5
11.0	64.3	152.5	97.5	16.6	7.0
10.1	63.5	165.6	132.0	21.0	8.0
6.4	51.7	152.9	76.5	9.4	3.2
15.7	106.4	282.9	102.0	15.0	5.7
43.1	271.2	706.7	134.4	21.3	8.2
1.2	7.6	19.2	182.8	29.0	11.5
2.5	16.1	41.0	86.4	13.5	5.3
5.8	31.3	68.5	200.0	37.0	16.9
10.0	65.4	173.6	143.9	23.5	9.6
145.6	5894.7	41293.6	6309.6	252.7	58.9

0	0
Branching frond SA (cm²)	Fronde plane SA (cm²)
73.2	20.5
435.0	68.0
1590.0	71.5
1047.1	37.6
1309.6	80.9
486.6	24.3
1599.8	37.3
5787.8	153.3
221.1	29.7
216.9	37.6
1151.8	85.1
1265.4	58.7
2563957.8	1522.7

Table S3. Fossil ranges

Assemblage	Formation	Country	Age (Ma)	Reference
Nama	Dabis	Namibia	547-541	Vickers-Rich et al 2013
White Sea	Zimnegory	Russia	555.3 ± 0.3	Grazhdankin 2004
White Sea	Verkhovka	Russia	558.3 ± 1	Grazhdankin 2004
Ediacara (White Sea)	Rawnsley Quartzite	Australia	556 ± 24	Geoscience Australia
Charnwood/Mercian (Avalon)	Bradgate - Beacon Hill	UK	563 ± 1.9	Wilby et al 2011
Avalon	Fermeuse	Canada		
Avalon	Trepassey	Canada	565 ± 3	Narbonne et al 2009
Avalon	Mistaken Point	Canada	565 ± 3	Narbonne et al 2009
Avalon	Briscal	Canada		
Avalon	Drook	Canada	575	Narbonne et al 2009

<i>Avalofractus abaculus</i>	Reference	<i>Beothukis mistakensis</i>	Reference	<i>Bradgatia linfordensis</i>
------------------------------	-----------	------------------------------	-----------	-------------------------------

present	Narbonne et al 2009	present	Narbonne et al 2009	present
		present	Narbonne et al 2009	present
		present	Narbonne et al 2009	present
		present	Brasier & Antcliffe 2009	present
		present	Narbonne et al 2009	present

Reference	<i>Charnia masoni</i>	Reference	<i>Culmofrons plumosa</i>	Reference
-----------	------------------------------	-----------	----------------------------------	-----------

	present	Narbonne & Gehling 2003		
Gehling & Droser 2013	present	Nedin & Jenkins 1998		
Flude & Narbonne 2008	present	Wilby et al 2011		
Flude & Narbonne 2008	present	Narbonne et al 2009		
Flude & Narbonne 2008	present	Narbonne et al 2009	present	Laflamme et al 2012
Flude & Narbonne 2008	present	Narbonne et al 2009	present	Laflamme et al 2012
	present	Liu et al 2012		

<i>Fractofusus andersoni</i>	Reference	<i>Fractofusus misrai</i>	Reference	<i>Hapsidophyllas flexibilis</i>
-------------------------------------	-----------	----------------------------------	-----------	---

present	Gehling & Narbonne 2007			
present	Gehling & Narbonne 2007	present	Gehling & Narbonne 2007	present
present	Gehling & Narbonne 2007			

Reference	<i>Pectinifrons abyssalis</i>	Reference	<i>Rangea schneiderhoehni</i>
			present
			present
			present

Bamforth & Narbonne 2009	present	Bamforth et al 2008
	present	Bamforth et al 2008

Reference	<i>Trepassia wardae</i>	Reference
Grazhdankin & Seilacher 2005		
Grazhdankin 2004		
Grazhdankin 2004		
	present	Narbonne et al 2009
	present	Narbonne et al 2009
	present	Narbonne & Gehling 2003

Supporting Video Legends

Video S1. Video animation of the L-system growth model for *Beothukis mistakensis*.

Video S2. Video animation of the L-system growth model for *Charnia masoni*.

Video S3. Video animation of the L-system growth model for *Hapsidophyllas flexibilis*.

Supporting References

45. Brasier MD, Antcliffe JB (2009) Evolutionary relationships within the Avalonian Ediacara biota: new insights from laser analysis. *J Geol Soc London* 166: 363-384.
46. Braybrook SA, Kuhlemeier C (2010) How a plant builds leaves. *The Plant Cell* 22:1006-1018.
47. Grazhdankin D (2004) Patterns of distribution in the Ediacaran biotas: facies versus biogeography and evolution. *Paleobiology* 30:203-221.
48. Wilby PR, Carney JN, Howe MPA (2011) A rich Ediacaran assemblage from eastern Avalonia: evidence of early widespread diversity in the deep ocean. *Geology* 39:655-658.
49. Bamforth EL, Narbonne GM (2009) New Ediacaran rangeomorphs from Mistaken Point, Newfoundland, Canada. *J Paleont* 83:897-913.
50. Bamforth EL, Narbonne GM, Anderson MM (2008) Growth and ecology of a multi-branched Ediacaran rangeomorph from the Mistaken Point assemblage, Newfoundland. *J Paleont* 82:763-777.
51. Grazhdankin D, Seilacher A (2005) A re-examination of the Nama-type Vendian organism *Rangea schneiderhoehni*. *Geol Mag* 142:571-582.
52. Dzik J (2002) Possible ctenophoran affinities of the Precambrian "sea-pen" *Rangea*. *J Morphol* 252:315-334.